Published OnlineFirst March 18, 2019; DOI: 10.1158/1541-7786.MCR-18-0315

Metabolism

Molecular Cancer Research

Adaptation to HIF1α Deletion in Hypoxic Cancer Cells by Upregulation of GLUT14 and Creatine Metabolism

Alessandro Valli[1,2], Matteo Morotti[1], Christos E. Zois[1], Patrick K. Albers[3], Tomoyoshi Soga[4], Katharina Feldinger[1], Roman Fischer[2], Martin Frejno[2], Alan McIntyre[1], Esther Bridges[1], Syed Haider[1], Francesca M. Buffa[1], Dilair Baban[3], Miguel Rodriguez[5,6], Oscar Yanes[5,6], Hannah J. Whittington[7], Hannah A. Lake[7], Sevasti Zervou[7], Craig A. Lygate[7], Benedikt M. Kessler[2], and Adrian L. Harris[1]

Abstract

Hypoxia-inducible factor 1α is a key regulator of the hypoxia response in normal and cancer tissues. It is well recognized to regulate glycolysis and is a target for therapy. However, how tumor cells adapt to grow in the absence of HIF1α is poorly understood and an important concept to understand for developing targeted therapies is the flexibility of the metabolic response to hypoxia via alternative pathways. We analyzed pathways that allow cells to survive hypoxic stress in the absence of HIF1α, using the HCT116 colon cancer cell line with deleted HIF1α versus control. Spheroids were used to provide a 3D model of metabolic gradients. We conducted a metabolomic, transcriptomic, and proteomic analysis and integrated the results. These showed surprisingly that in three-dimensional growth, a key regulatory step of glycolysis is Aldolase A rather than phosphofructokinase. Furthermore, glucose uptake could be maintained in hypoxia through upregulation of GLUT14, not previously recognized in this role. Finally, there was a marked adaptation and change of phosphocreatine energy pathways, which made the cells susceptible to inhibition of creatine metabolism in hypoxic conditions. Overall, our studies show a complex adaptation to hypoxia that can bypass HIF1α, but it is targetable and it provides new insight into the key metabolic pathways involved in cancer growth.

Implications: Under hypoxia and HIF1 blockade, cancer cells adapt their energy metabolism via upregulation of the GLUT14 glucose transporter and creatine metabolism providing new avenues for drug targeting.

Introduction

Highly proliferating cancer cells must increase the import of nutrients and adopt a metabolic program that fulfils energetic, redox, and biosynthetic requirements for increasing cell mass. Metabolic flexibility is acquired through genetic and nongenetic factors that allow tumors to grow in altered biochemical conditions such as hypoxia, acidic pH, and a nutrient-poor microenvironment (1).

Warburg first described the increase of oxidation of glucose into lactate in cancer cells (2). Although yielding less ATP than OXPHOS, glycolysis is utilized predominantly by cancer cells and provides a more rapid response to the high energy demand of rapidly proliferating cancer cells (3). In hypoxia, this regulation represents the predominant way to produce ATP, even for normal cells (1). Although many solid tumors demonstrate the Warburg effect, some, such as prostate cancer, do not (4). Virus-infected cells show increased glucose metabolism and $CD4^+$ T-cell growth is characterized by a high synthesis of ATP and biosynthetic reactions (cell membrane and DNA biosynthesis). These observations show that uncoupling glycolysis from OXPHOS can offer a metabolic solution adequately beneficial for the high energy demand while maintaining redox balance and biosynthetic requirements (5–7). Similarly, reprogramming of cancer metabolism activates distinct pathways in which oncogenic mutations convey downstream signals to directed prometabolic traits (1).

Adaptation to the hypoxic tumor microenvironment is driven by hypoxia-inducible factors HIF1α and HIF2α that induce a distinct transcriptional program (8). HIF1α regulates numerous metabolic genes, especially those involved in glycolysis and related auxiliary processes (9).

Because of the importance of HIF1 in tumor growth and the potential of HIF1α as target, we investigated how a cell line

[1]Weatherall Institute of Molecular Medicine, University of Oxford, Oxford, United Kingdom. [2]Target Discovery Institute, Nuffield Department of Medicine, University of Oxford, Oxford, United Kingdom. [3]The Wellcome Trust Centre for Human Genetics, University of Oxford, Oxford, United Kingdom. [4]Institute for Advanced Biosciences, Keio University, Tsuruoka, Yamagata, Japan. [5]Metabolomics Platform, IISPV, Department of Electronic Engineering, Universitat Rovira i Virgili, Tarragona, Spain. [6]Spanish Biomedical Research Center in Diabetes and Associated Metabolic Disorders-CIBERDEM, Madrid, Spain. [7]Division of Cardiovascular Medicine, Radcliffe Department of Medicine, University of Oxford, Oxford, United Kingdom.

Note: Supplementary data for this article are available at Molecular Cancer Research Online (http://mcr.aacrjournals.org/).

B.M. Kessler and A.L. Harris are the co-senior authors of this article.

Corresponding Author: Alessandro Valli, University of Oxford, Oxford OX3 9DS, United Kingdom. Phone: 4418-6522-2420; Fax: 4418-6522-2431; E-mail: alevalli14@gmail.com and alessandro.valli@cardiologicomonzino.it

Mol Cancer Res 2019;17:1531–44

doi: 10.1158/1541-7786.MCR-18-0315

Published OnlineFirst March 18, 2019; DOI: 10.1158/1541-7786.MCR-18-0315

deleted for HIF1α could survive in hypoxia. We studied the HCT116 colorectal cancer cell line wild-type (WT) and HIF1α knockout (KO) under hypoxic conditions and analyzed transcriptomics, proteomics, metabolomics, and fluxomics. We integrated the multi-omics data to construct a map of hypoxic colorectal cancer cell energy metabolism. Our results show for the first time upregulation of glucose transporter type 14 (GTR14) to maximize nutrient uptake and an important role for creatine (Cr) energy pathways to sustain multidimensional growth under hypoxic conditions.

Materials and Methods

Cell culture

Cell lines were available from Clare Hall Laboratories (HCT116), or were a kind gift from Prof Walter Bodmer (Weatherall Institute of Molecular Medicine, Oxford, United Kingdom; DLD-1, Ls174T). Cell line authentication was carried out by short tandem repeat analyses (LGC Standards) 6 months prior to the first submission of the manuscript. Cells were cultured as described previously, unless different conditions were specified (10).

Enzyme activity assay

WT and KO HCT116 cells were cultivated at either 21% O_2 or 1% O_2 for 24 hours. Cells were collected, pelleted, and suspended in 1 mL of ice-cold buffer (0.08 mmol/L K_2HPO4, 1 mmol/L EGTA, 0.02 mmol/L KH_2PO_4, and 1 mmol/L β-mercaptoethanol) while under experimental conditions. Samples were vortexed and 150 μL aliquots removed for determination of protein by the Lowry method. A final concentration of 0.1% v/v Triton X-100 was added to permeabilize cells. Samples were stored on ice for at least 30 minutes to allow precipitation and the supernatant was used for all enzyme activity measurements.

Total creatine kinase activity

Twenty microliters of 1:5 (in ice buffer) diluted sample supernatant was incubated with 1 mL of creatine kinase (CK)-NAC reagent (Thermo Fisher Scientific) at 30°C. After 3-minute lag time, CK activity was quantified spectrophotometrically by measuring the increase in absorbance at 340 nm over 2 minutes as a result of NADH production. The assay was performed in triplicate and results normalized to protein concentration.

Relative activity of creatine kinase isoenzymes

Sample supernatant was diluted 1:200 in ice buffer and incubated with 1% CK isoenzyme activator for 10 minutes prior to use. Creatine kinase isoenzymes were separated according to their electrophoretic mobility on an agarose gel, followed by incubation with CK isoenzyme chromogen, which allowed visualization of the bands. Relative activities of individual CK isoenzymes were quantified by densitometry. All reagents were provided within the SAS-1 CK VIS-12 Isoenzyme Kit (Helena Biosciences). Absolute activities for each isoenzyme were calculated by multiplying relative isoenzyme activity by total CK activity.

Citrate synthase activity

Fifty microliters of sample supernatant was incubated with 850 μL of reaction mixture (0.35 mmol/L acetyl-CoA, 0.12 mmol/L DTNB) at 25°C. After 3 minutes, 100 μL of 1 mmol/L oxaloacetate was added into the reaction mixture. Citrate synthase (CS) activity was immediately assessed spectrophotometrically by measuring the increase in absorbance at 412 nm over 1 minute as a result of 5-thio-2-nitrobenzoate (TNB2-) production. The assay was performed in duplicate and results were normalized by protein concentration.

Results

HIF1α regulates hypoxic spheroid cancer growth

We cultured WT and KO HCT116 cells as spheroids (WTs and KOs) for 72 hours, generating a hypoxic inner mass, and evaluated their morphology at three time points (72.5, 76, and 96 hours). Immunostaining of WTs and KOs spheroids at 96 hours showed key differences in hypoxic adaptation. Pimonidazole (PIMO)-positive staining, in both WTs and KOs, confirmed the presence of hypoxic areas, and carbonic anhydrase 9 (CA9; HIF1α-target) positive stain in WTs demonstrated the presence of hypoxia and HIF1α stabilization. In contrast, CA9 staining was absent in KOs, demonstrating successful HIF1α knockout. Necrosis and cell death, as measured by H&E staining, was more pronounced in WTs than in KOs (Fig. 1A).

We evaluated differences in growth of WTs and KOs (Fig. 1B). HCT116 WTs and KOs proliferated over 24 hours, with a higher rate in WTs (top). WTs volume was overall significantly bigger than that of KOs cells with no marked changes over time (middle). Cell spheroid density (number of cells per spheroid/spheroid volume) showed a significant increased over time in both WTs and KOs and was more pronounced in KOs at 96 hours (bottom).

HIF1α metabolic effects in cancer spheroids

Because WTs and KOs grow unequally, we optimized the formation of WTs and KOs with a comparable cell number, morphology, volume, and diameter, which enabled the investigation of hypoxic gradients at the studied time points (72.5, 76, and 96 hours; data not shown). We measured 26 metabolites of six metabolic pathways: glycogen (GLG), glycolysis (GLY), TCA cycle, ATP, Cr, and redox metabolism (Fig. 1C). GLG metabolic intermediates show a general decrease over time in both WTs and KOs. Glycolysis and Cr metabolic products accumulated mostly in WTs. TCA cycle metabolites did not show a defined trend, but generally appeared to be more elevated in WTs at 96 hours and decreased in KOs over time. We observed higher amounts of ATP in WTs versus KOs, and this difference remained stable over time; ADP levels decreased at 96 hours in both in WTs and KOs. NAD^+ levels were low overall, while ADP and AMP were lower in KOs versus WTs. HIF1α deletion correlated with higher AMP compared with ATP, but with less difference over time (Fig. 1D). Supplementary Figure S1 shows statistical results for the metabolites detected in WTs and KOs.

Glycolytic and TCA flux in spheroids in hypoxia without HIF1α

We next evaluated glycolysis and TCA cycle flux in spheroids in the presence and absence of HIF1α. Spheroids were grown for 72 hours and we utilized $^{13}C_6$ Glucose (Glu) for metabolic flux analysis (MFA; Fig. 2A). We calculated the isotopolog ratio for each metabolite as [single fully labeled isotopolog value]/[sum of the total isotopolog value] ratio (STIR). Next, we evaluated glycolysis and TCA STIR distribution. We noted that the overall STIR range was wider for metabolites of glycolysis compared with the TCA cycle (STIR glycolysis 0.2–0.8; STIR TCA cycle: 0.3–0.45).

In glycolytic MFA (Fig. 2B), Glu 6 phosphate (Glu-6P) STIR increased linearly in WTs between 72.5 and 96 hours, increased

Published OnlineFirst March 18, 2019; DOI: 10.1158/1541-7786.MCR-18-0315

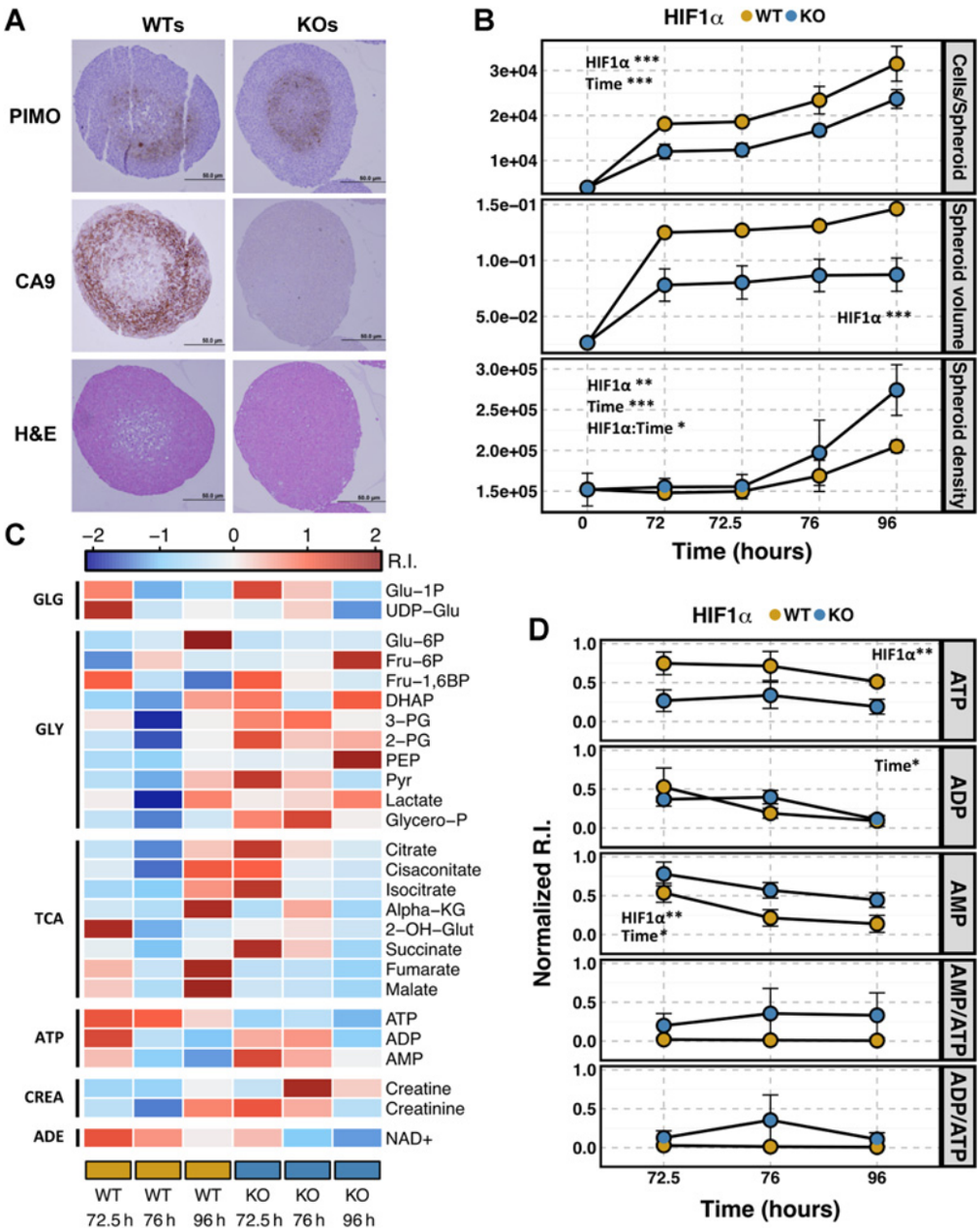

Figure 1.

Spheroid hypoxic phenotype and energy metabolism. **A,** Immunostaining of spheroids for protein expression of hypoxic markers. PIMO, CA9, and H&E expression in spheroids formed with HCT116 colorectal cancer cells HIF1α (WT) and HIF1α-deficient (KO). **B,** HIF1α WT and KO spheroid morphology. Spheroid-forming cell count (cell number, top), spheroid volume (cm^3, middle), and spheroid cell density (cell number/spheroid volume ratio, bottom). **C,** Heatmap showing z-normalized intensities of energy-related metabolites in WT and KO spheroids at time points 72.5, 76, and 96 hours after formation. R.I., Relative intensity. **D,** Specific ATP, ADP, AMP, ATP/AMP ratio, and ATP/ADP ratio relative intensities (R.I. 0–1 normalized) in WT and KO spheroids at time points 72.5, 76, and 96 hours after formation. Metabolic pathways: glycogen (GLG), glycolysis (GLY), Krebs cycle (TCA), adenosine triphosphate (ATP), creatine (Cr), and oxidation–reduction (REDOX). Data are reported as average ± SD ($N = 3$). Statistical comparisons were performed using two-way ANOVA, multiple *post hoc* group comparisons, or *t* test (*P* values corrected for multiple testing using the Benjamini–Hochberg procedure at $\alpha = 1\%$), showing *P* value <0.05 (*), <0.01 (**), and <0.001 (***).

significantly in WTs versus KOs at 96 hours, but remained stable in KOs. No effect was observed on $^{13}C_6$ fructose 6 phosphate (Fru-6P) MFA. Fructose 1, 6 bis phosphate (Fru-1,6BP) STIR decreased linearly in WTs between 72.5 and 96 hours, but remained stable in KOs. No effect was observed on $^{13}C_6$ dihydroxyacetone phosphate (DHAP), 3-phosphoglycerate (3-PG), 2-phosphoglycerate (2-PG), and phosphoenolpyruvate (PEP) MFA in either spheroid type. Pyruvate (Pyr) and

Published OnlineFirst March 18, 2019; DOI: 10.1158/1541-7786.MCR-18-0315

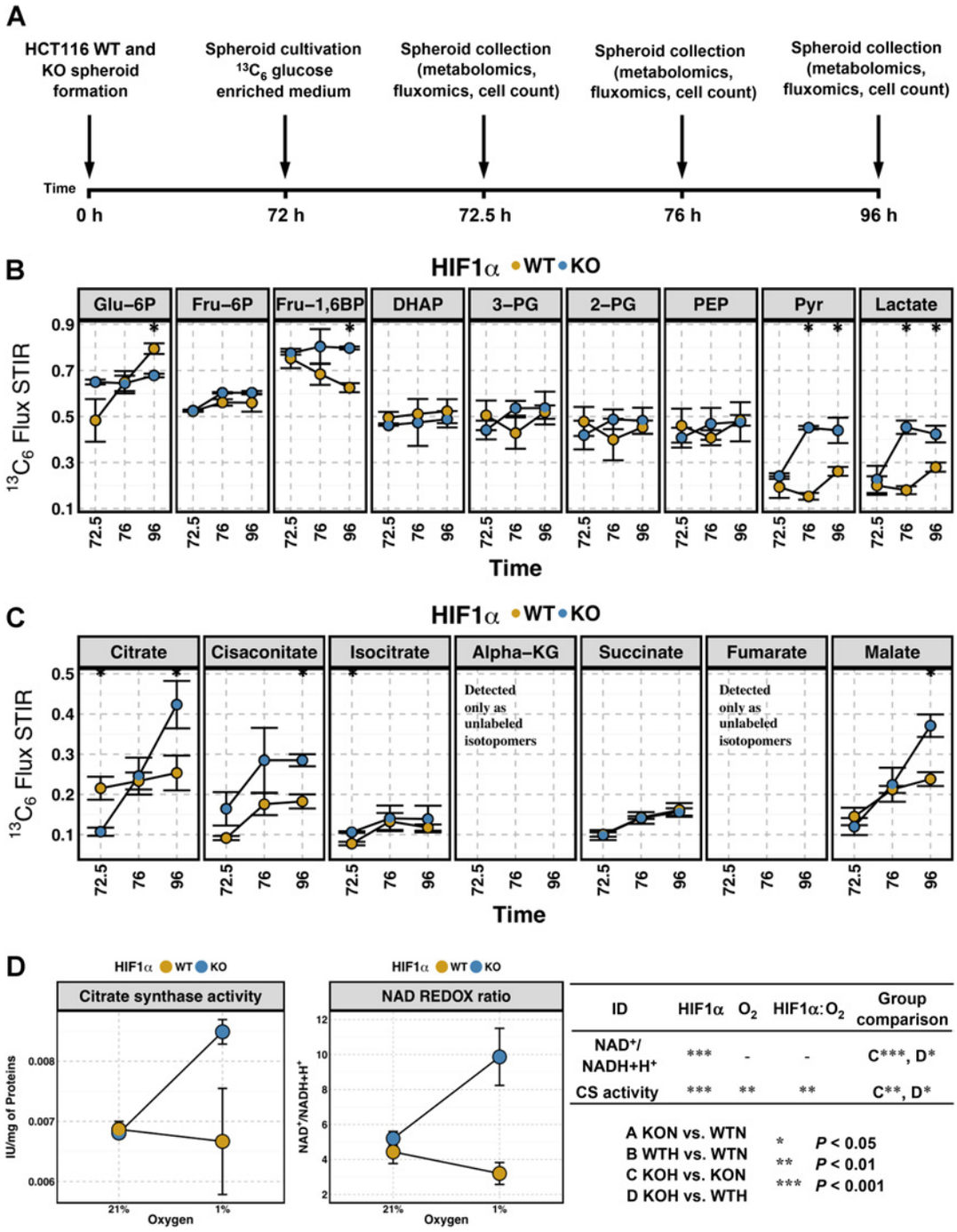

Figure 2.

Metabolic flux in spheroids. **A,** Experimental design of metabolomics flux analysis in spheroids. **B** and **C,** Glycolytic and TCA metabolic flux analysis after administration of $^{13}C_6$ glucose. Isotopolog quantification is shown by STIR ratio [single fully labeled isotopolog value]/[sum of the total isotopolog value]. **D,** NAD^+/ $NADH+H^+$ ratio and CS activity and WTN, KON, WTH, and KOH cell proliferation after 24 hours in two O_2 conditions (21% and 1%). Data are reported as average ± SD ($N = 3$). Statistical comparisons were performed using two-way ANOVA, multiple *post hoc* group comparisons or *t* test (*P* values corrected using the Benjamini–Hochberg procedure at $\alpha = 1\%$), showing *P* value <0.05 (*), <0.01 (**), and <0.001 (***).

lactate STIR levels increased in WTs 96 hours versus earlier time points, whereas they accumulated earlier and to higher levels (76 hours) in KOs.

In the TCA MFA (Fig. 2C), citrate STIR showed a linear increase in KOs. It was significantly lower in KOs than in WTs at 72.5 hours and became significantly higher at 96 hours, whereas citrate STIR

Published OnlineFirst March 18, 2019; DOI: 10.1158/1541-7786.MCR-18-0315

remained stable in WTs. These data matched CS activity and its allosteric enzymatic regulator $NAD^+/NADH+H^+$ ratio both of which showed a significant increase only in HCT116 KO hypoxic cells (KOH; Fig. 2D).

Cis-aconitate, isocitrate, and succinate STIR was essentially unchanged, but *cis*-aconitate accumulated in KOs at 96 hours. Alpha-KG and fumarate STIR were not assessed as only the unlabeled isotopologs were detected. Malate STIR increased linearly in KOs between 72.5 and 96 hours and was significantly higher than in WTs at 96 hours. Malate STIR showed a mild increase between 72.5 and 96 hours in WTs (Fig. 2C).

Thus, glucose uptake was maintained without HIF1α and a clear block of conversion of Fru-1,6BP to DHAP occurred without HIF1α, at aldolase level, rather than the earlier step of conversion by phosphofructokinase of Fru-6P to Fru-1,6BP. There was, in addition, a surprising higher lactate and Pyr without HIF1α.

Because of this unexpected effect in the aldolase step on the glycolytic flux, we evaluated the clinical relevance of aldolase in colorectal cancer. We investigated whether tumor ALDOA mRNA expression levels correlated with patient prognosis using overall survival data derived from a cohort of 440 colon adenocarcinoma patients (The Cancer Genome Atlas). We found that, when the patient group was divided in quartiles, the highest quartile had a reduced 5-year survival (Kaplan–Meier analysis of overall survival; log-rank $P < 0.05$; Supplementary Fig. S2A).

HIF response in 2D growth

For further manipulations of the cells, we used 2D growth. We initially confirmed the biology for HCT116 WT and KO cells in normoxia (N) and hypoxia (H; WTN, KON, WTH, and KOH; ref. 10). Hypoxia reduced proliferation in WTH and KOH cells, and the lack of HIF1α reinforced this effect in both normoxia and hypoxia (Fig. 3A). We observed no difference in cell proliferation when experiments were conducted in 5 mmol/L or 25 mmol/L Glu (data not shown). HIF1α expression was barely detectable in WTN, strongly accumulated in WTH, and was absent in both KON and KOH. CA9 accumulated only in WTH. HIF2α doubled in expression in both WTH and KOH versus WTN and KON, showing no notable compensatory effect in the absence of HIF1α (Fig. 3B). In the 2D experiments, we detected 27 metabolites (Figs. 3C and 4A), 86 proteins (Figs. 3D and E and 4B and C), and 76 mRNAs (Fig. 4D) involved in ATP metabolism and related metabolic pathways that involve GLG, GLY, TCA cycle, ATP, Cr, redox, and adenosyl metabolism. We observed the highest ATP level in WTN. Both hypoxia and lack of HIF1α lowered ATP in a cumulative fashion. Intracellular ADP did not show any significant differences. There was a significant increase in AMP levels in hypoxia, with the effect reinforced by the lack of HIF1α in KOH (Fig. 4E).

Analysis of metabolome. More small molecules accumulated in WTH and in KOH than in WTN and KON. Metabolites increased in WTH versus WTN were GLG, Glu, Glu-6P, 2-PG, lactate, and NAD^+. Fumarate and malate were significantly increased in WTN. Comparing WTH versus KOH cells, a set of metabolites increased in KOH (Glu-1P, UDP-Glu, Fru-1,6BP, lactate, succinate, fumarate, malate, AMP, Cr). We assessed intracellular levels of PCr and Cr and calculated PCr/Cr ratio. We observed a decrease in ratio in WTH versus KOH ($P < 0.01$); in addition, in both WTH and KOH, the ratios were decreased versus their parental normoxic cells WTN and KON ($P < 0.001$; Supplementary Fig. S6A and S6B). Lactate levels were significantly increased in WTH when compared with WTN and further increased in KOH when compared with WTH, matching to the 3D flux (Figs. 2B and 4A). TCA metabolites were elevated in KOH demonstrated the predominant role of HIF1α in redirecting metabolism away from TCA cycle in hypoxia (Figs. 3C and 4A).

Analysis of proteome. Many previously described enzymes were increased in WTH versus WTN (e.g., PGM1, GLGB, GTR1, HEXK1, G6PI, and PFKAM). Comparing WTH versus KOH cells, enzymes were similarly elevated in the WTH, demonstrating the predominant role of HIF1α (PGM1, GLGB, GTR1, G6PI, and PFKAM).

In contrast, in KOH versus WTH, UGPAse, GYS1, GTR3/GTR14 (proteomics did not differentiate between the two transporters), PFKAL, PFKAP, PDP1, PDPR, ACLY, IDH3G, ADT2, ATAD2, KCRB, BLVRB, and ADK were upregulated. TIGAR was upregulated (but decreased in WTH vs. WTN; Figs. 3D and E and 4B and C).

Analysis of transcriptome. We next evaluated mRNA features associated with the targeted proteomics signature. In WTH versus WTN, we observed an increase of *GLGB*, *GSK3B*, *GTR1*, *GTR3*/*GTR14*, *HEXK1*, *PFKAL*, *ALDOA*, *PGK1*, *PGAM1*, *ACON*, and many others. *PYGB*, *PDRP*, *IDH3A*, and *AAPK1* were downregulated.

When we evaluated KOH versus WTH, we observed *PYGB*, *UGPAse*, *GTR3* and/or *GTR14*, *TIGAR*, *FUMH*, *ATPD*, *ATAD2*, *BLVRB*, and *AAPK1* upregulated. However, most of the genes were lower (*GTR1*, *PGM2*, *GLGB*, *GSK3B*, *GTR1*, *G6PI*, *PGK1*, *PGAM1*, *PKM*, *ACON*, *IDH3G*, *KCRU*, and *KAD4*; Fig. 4D).

HIF1α and hypoxia-dependent effects on transcription and protein levels

We correlated transcriptomics and proteomics by calculating for each feature $\log_2$ fold changes (FC) for mRNA and proteins comparing the following models: KON-WTN (HIF1α effect in normoxia), WTH-WTN (HIF1α effect in hypoxia), KOH-KON (HIF1α-independent hypoxia effects), and KOH-WTH (HIF1α effect in hypoxia, expected to be similar to WTH-WTN).

We applied linear regression analysis to correlate mRNA $\log_2$ FC and protein $\log_2$ FC for each model. The correlation of WTN-WTH was similar to KOH-WTH. In contrast, KOH versus KON showed no significant correlation. Interestingly, there was strong evidence for a normoxic effect of HIF1α as the slope for KON versus WTN was similar to that for KOH versus WTH (Supplementary Fig. S3).

Significantly regulated genes at either RNA and protein level (63 for WTH-WTN and 56 for KOH-WTH) were compared to evaluate transcription and/or translation patterns of regulation under hypoxia.

They are shown (protein and mRNA) in a heatmap of $\log_2$ FC. For many previously well-characterized genes, there was a close correlation of mRNA and protein, but in some proteins went up proportionally more (ACON, ATP5J, ATAD2, GTR14) suggesting a stronger posttranslational element. In others, mRNA increased without a change in protein (GSK3B and TIGAR). The most regulated features were selected on the basis of residuals below and above -2σ and 2σ distribution for each experimental condition (Fig. 4D; Supplementary Fig. S3).

Protein kinase AMPK expression showed a significant increase only in WTH versus WTN (50%, $P < 0.01$). Interestingly, p-AMPK

Published OnlineFirst March 18, 2019; DOI: 10.1158/1541-7786.MCR-18-0315

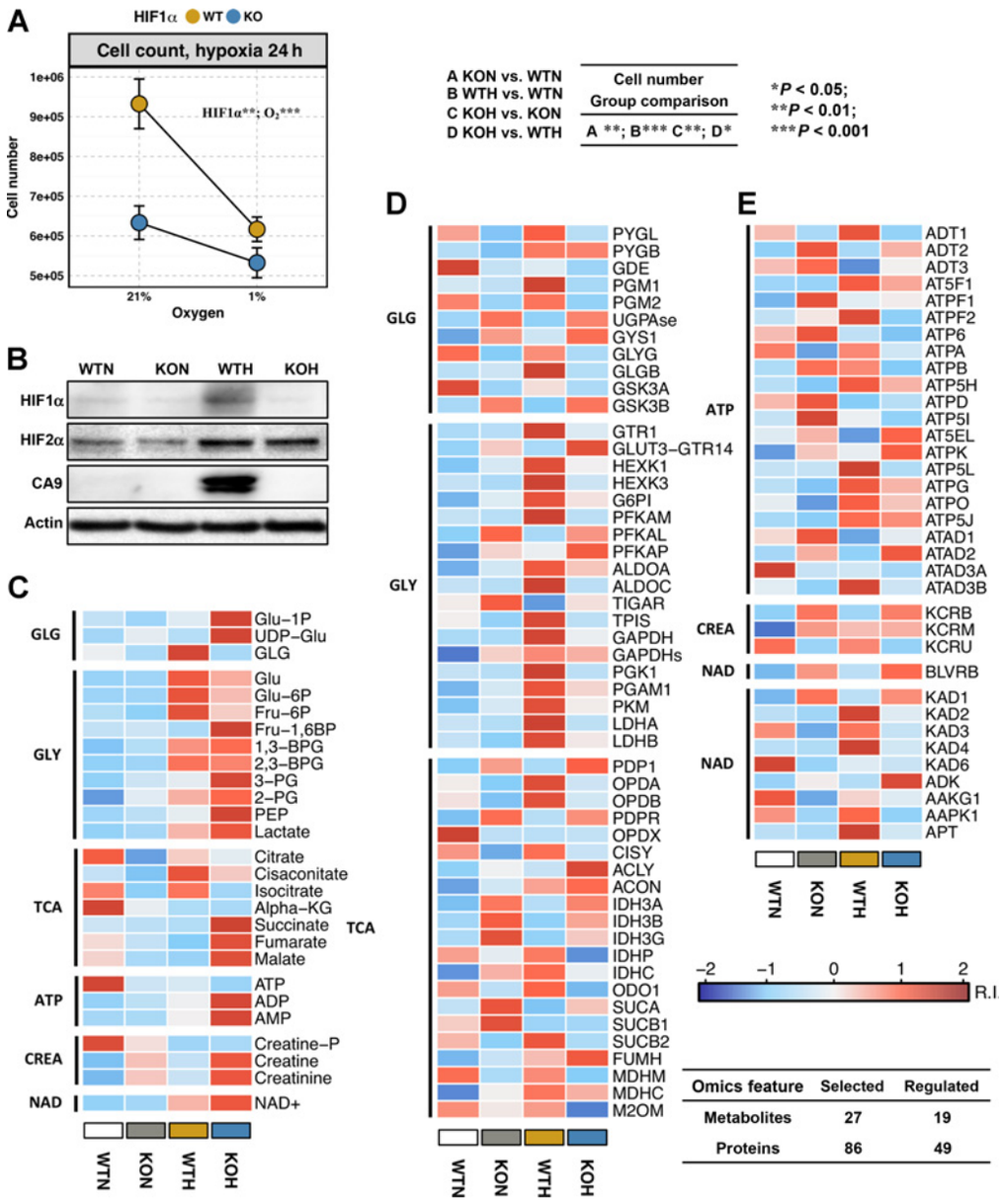

Figure 3.

Proteo-metabolomics profile of hypoxic HCT116. **A,** WTN, KON, WTH, and KOH cell proliferation after 24 hours in two O_2 conditions (21% and 1%). **B,** Western blot analysis showing HIF1α stabilization in hypoxia and successful deletion in KO HCT116 cells. HIF1α, HIF2α, and CA9 protein expression in cells: HIF1α wild-type normoxia (WTN), HIF1α-deficient normoxia (KON), HIF1α wild-type hypoxia (WTH), and HIF1α-deficient hypoxia (KOH). **C–E,** Proteo-metabolomics heatmaps (**C** metabolites; **D** and **E** proteins) of the detected metabolites and proteins in WTN, KON, WTH, and KOH cells after 24-hour exposure to two O_2 conditions (21% and 1%). Normalized levels refer to WTN. R.I., Relative intensity. Metabolic pathways: glycogen (GLG), glycolysis (GLY), Krebs cycle (TCA), adenosine triphosphate (ATP), creatine (Cr), oxidation–reduction (REDOX), and adenosyl metabolism. Data are reported as average ± SD ($N = 3$). Statistical comparisons were performed using two-way ANOVA, multiple *post hoc* group comparisons, or *t* test, showing *P* value <0.05 (*), <0.01 (**), and <0.001 (***).

was strongly expressed in the absence of HIF1α in both KON and KOH. AMPK/p-AMPK (levels normalized by β-actin) ratio was positive for KON and KOH, (13 and 9, respectively) while it was negative for WTN and WTH (Supplementary Fig. S6C).

HIF1α/HIF2α hypoxic interaction regulates GTR14 expression

Flux analysis highlighted that Glu uptake was maintained in the absence HIF1α; thus, we studied in more detail Glu transporters in hypoxia. PCR analysis showed GTR3 and GTR14 more highly expressed in the absence of HIF1α in normoxia. Both genes were induced in WT cells in hypoxia, but more highly induced in the KO cells, KOH (Fig. 5A and B). Similar results were observed for more severe hypoxia O_2 0.1% (Supplementary Figs. S4A and S5A) and in two other colorectal cancer cell lines DLD1 (Supplementary Figs. S4B and S5B), and Ls174T (Supplementary Figs. S4C and S5C).

Published OnlineFirst March 18, 2019; DOI: 10.1158/1541-7786.MCR-18-0315

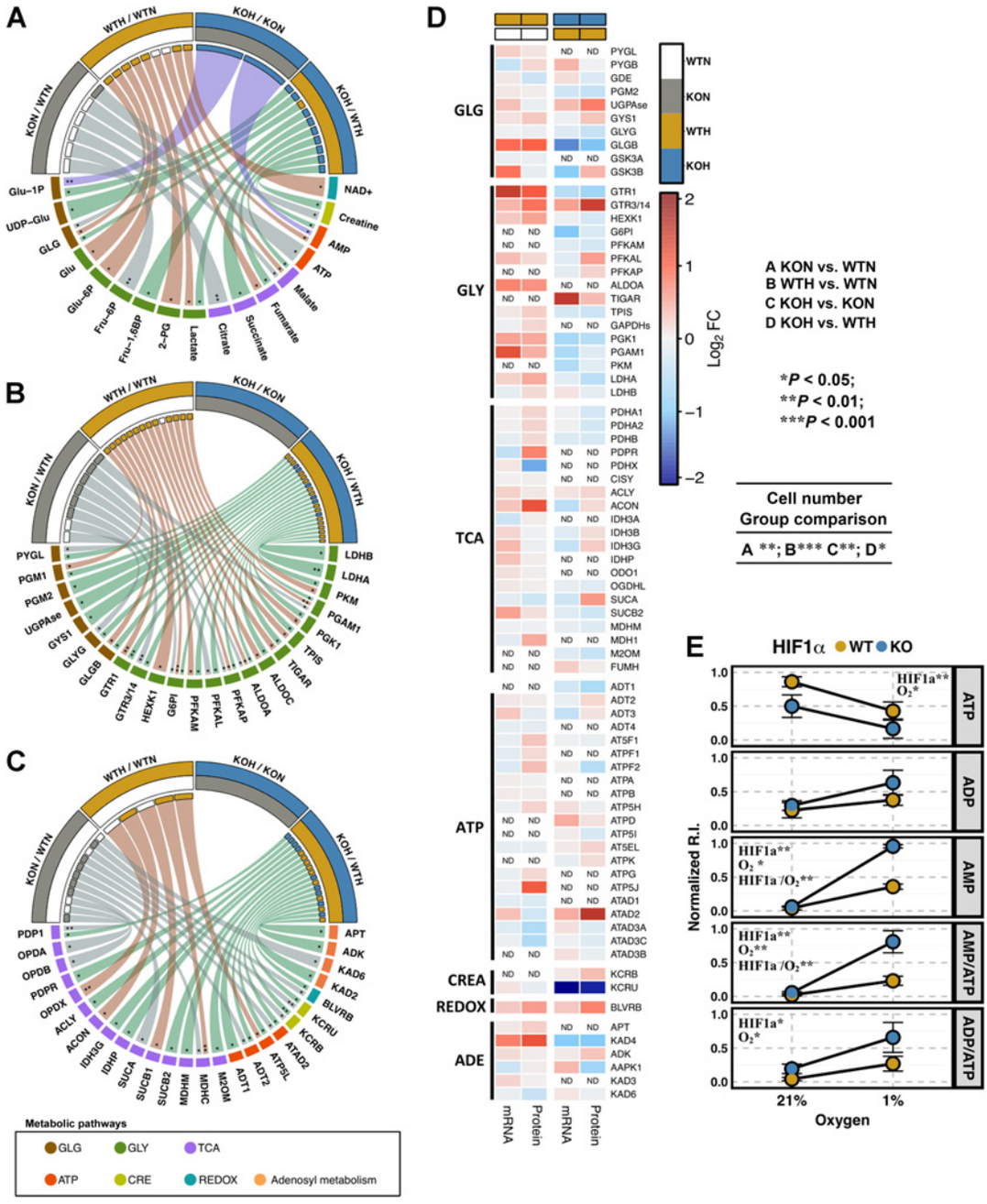

Figure 4.

Analysis of the HCT116 hypoxic metabolic phenotype. **A–C,** Metabolomics- and proteomics-integrated circos-plots showing significantly regulated features only in KON versus WTN, WTH versus WTN, KOH versus KON, and KOH versus WTH (upper side circos-plots). Adjusted $P < 0.05$ (*) or $P < 0.01$ (**) are indicated for the different experimental comparisons (connecting lines inside circos-plots): KON/WTN (gray/white-gray connection) WTH/WTN (gold/white-brown connection), KOH/KON (blue/gray-violet connection), KOH/WTH (blue/gold-green connection). Colored boxes (lower side circos-plots linked to connecting lines) represent different metabolic pathways, while colored boxes (inside circos-plots linked to connecting lines) identify the biological condition where the feature is upregulated. **D,** Heatmap of integrated transomics (proteomics and transcriptomics); mRNA and protein $\log_2$ FC are calculated for WTH-WTN and KOH-WTH. Feature selection was based on departure from 95% confidence intervals of the linear model distribution built for each comparison (WTH-WTN and KOH-WTH). Metabolic pathways: glycogen (GLG), glycolysis (GLY), Krebs cycle (TCA), adenosine triphosphate (ATP), creatine (Cr), oxidation–reduction (REDOX), and adenosyl metabolism (ADE). **E,** Targeted metabolomics showing distribution of ATP, ADP, AMP, ATP/AMP, and ATP/ADP ratios in WTN, KON, WTH, and KOH cell after 24 hours in 21% and 1% O_2. Raw intensities and ratios are shown as 0–1 normalized levels' relative intensity (R.I). Data are reported as average ± SD ($N = 3$). Statistical comparisons were performed using two-way ANOVA, multiple *post hoc* group comparisons or *t* test (*P* values corrected using the Benjamini–Hochberg procedure at $\alpha = 1\%$), showing *P* value <0.05 (*), <0.01 (**), and <0.001 (***).

Published OnlineFirst March 18, 2019; DOI: 10.1158/1541-7786.MCR-18-0315

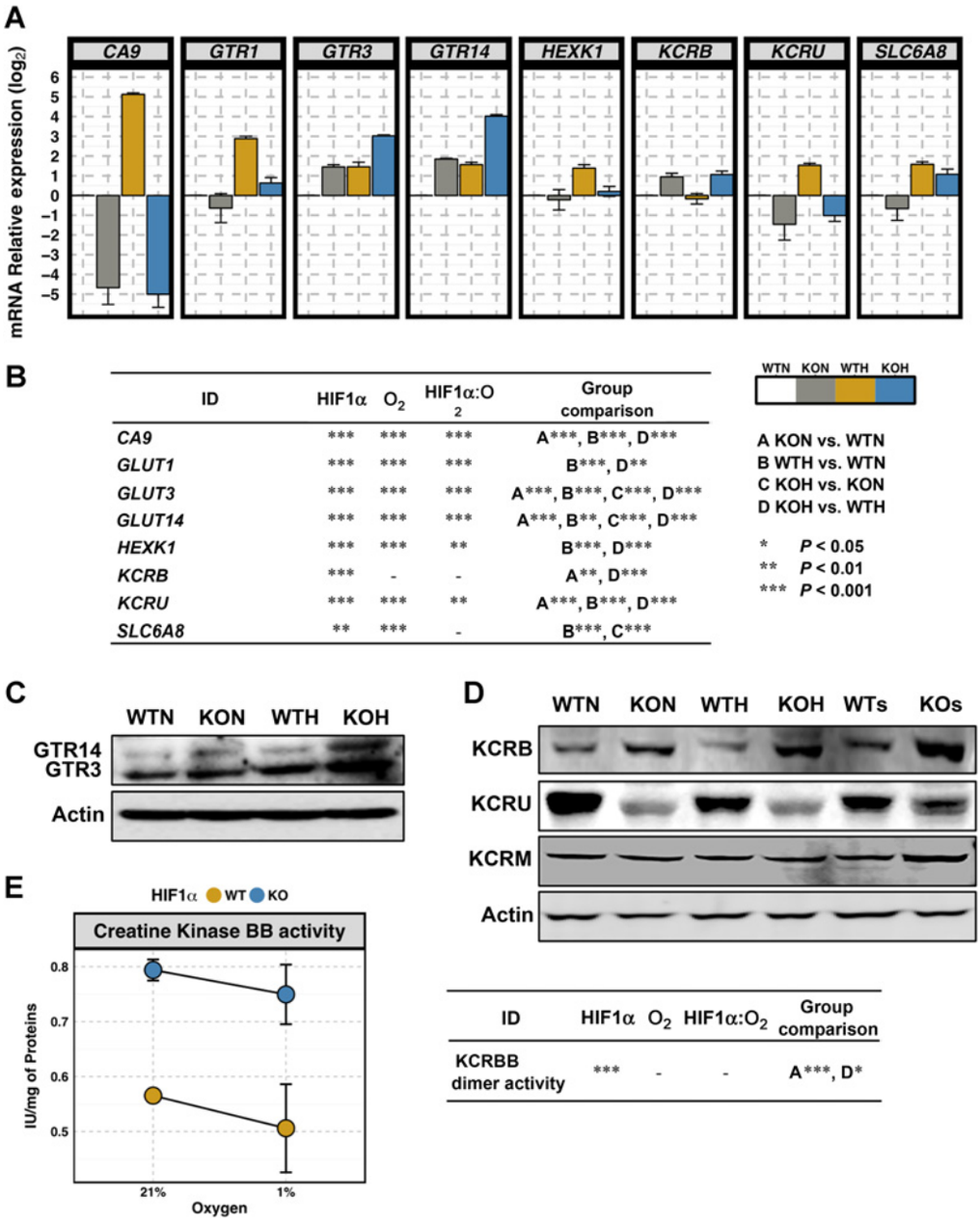

ID	HIF1α	O_2	HIF1α:O_2	Group comparison
CA9	***	***	***	A***, B***, D***
GLUT1	***	***	***	B***, D**
GLUT3	***	***	***	A***, B***, C***, D***
GLUT14	***	***	***	A***, B**, C***, D***
HEXK1	***	***	**	B***, D***
KCRB	***	-	-	A**, D***
KCRU	***	***	**	A***, B***, D***
SLC6A8	**	***	-	B***, C***

ID	HIF1α	O_2	HIF1α:O_2	Group comparison
KCRBB dimer activity	***	-	-	A***, D*

Figure 5.

Congruence between multi-omics metabolic reconstruction and hypoxia biochemistry. **A,** PCR analysis of CA9, GTR1, GTR3, GTR14, HEXK1, KCRU, KCRM, and SLC6A8 mRNA levels in WTN, KON, WTH, and KOH cells after 24-hour exposure to two O_2 conditions (21% and 1%). **B,** Statistical significance for PCR analysis–measured features. **C** and **D,** Western blot analysis of GTR14, GTR3, KCRB, KCRU, and KCRM in WTN, KON, WTH, and KOH cells after 24-hour exposure to two O_2 conditions (21% and 1%), and in WTs and KOs spheroids (96 hours). **E,** CK BB activity and WTN, KON, WTH, and KOH cell proliferation after 24-hour exposure to two O_2 conditions (21% and 1%). Data are reported as average ± SD ($N = 3$). Statistical comparisons were performed using two-way ANOVA, multiple *post hoc* group comparisons, or *t* test (*P* values corrected using the Benjamini–Hochberg procedure at $\alpha = 1\%$), showing *P* value <0.05 (*), <0.01 (**), and <0.001 (***).

Western blot analysis showed GTR3 induced mostly in KOH and slightly in WTH. GTR14 was suppressed by HIF1α in both WTN and WTH versus KON and KOH. Hypoxia, in absence of HIF1α, reinforced GTR14 expression protein as shown by KOH versus KON (Fig. 5C; Supplementary Fig. S4E).

We studied the effects of HIF1α and HIF2α on GTR14 modulation in hypoxia. We utilized HCT116 WT cells HIF1α and HIF2α single knockdown and HCT116 KO HIF2α knockdown exposed to 1% O_2 (WT1KDH, WT2KDH, KO2KDH). CA9 suppression in KON, WT1KDH, KOH, and KO2KDH versus WTN and WTH, confirmed HIF1α absence. HIF2α suppression in WT2KDH

Published OnlineFirst March 18, 2019; DOI: 10.1158/1541-7786.MCR-18-0315

and KO2KDH versus WTH, WTKD1H, and KOH, confirmed HIF2α knockdown (Supplementary Figs. S4D and S5D). *GTR1* RNA expression increased only in WTH and WT2KDH, that is, in response to HIF1α (Supplementary Figs. S4D and S5D). In normoxia, *GTR3* was higher in KO cells and further increased in the KOH. In hypoxia, the levels increased in WT cells to the same level as KON. However, HIF2α KD had only a small effect on the expression level in either cell line, suggesting that in the WT cells, it is mainly HIF1α regulated and the adaptation in KO cells is through a different pathway. Yet, in DLD1 cells, HIF2 is clearly the factor involved in *GTR3* regulation in hypoxia (Supplementary Fig. S4B).

GTR14 was higher in KON than in WTN, and in WTH increased to a similar but lower level than KON. KOH increased further than KON. WTKD1H had higher levels than WTH. Knockdown of HIF2 in the KO cells substantially reduced the high *GTR14* levels. These data support the potential role of HIF2α competing with HIF1, so that in absence of HIF1, a great effect of HIF2α occurs in hypoxia. Similar results were shown for DLD1 cells (Supplementary Fig. S4B), where HIF2α antagonized HIF1α and induction was greater with HIF1α KD, and ablated with HIF2α knockdown. In Western blot analysis of GTR3 and GTR14 (Supplementary Fig. S4E), KOH had the highest levels of GTR3 and 14, reduced by HIF2α KD, but not by HIF1α KD in WT cells, which had the lowest levels of both transporters. No effect on cell proliferation was observed when GTR3 was knocked down. However, GTR14 knockdown showed a significant decrease of cell proliferation (about 40% in WTN and KON $P < 0.001$; 50% WTH and KOH $P < 0.01$ and $P < 0.05$) after 24-hour cultivation in any of the studied experimental conditions, showing a high dependency of HCT116 on this glucose transporter (Supplementary Fig. S7A). FC in HCT116 cells' proliferation comparing normoxia and hypoxia upon GTR14 silencing in HIF1α-deficient and control cells showed significant reduction in KOH/WTH (FC = 0.3 ± 0.06) as compared with KON/WTN (FC = 0.6 ± 0.08, $P < 0.01$), WTH/WTN (FC = 0.5 ± 0.06, $P < 0.01$), and KOH/KON (FC = 0.6 ± 0.1, $P < 0.001$). Finally, there was a reduction in proliferation when HIF2α was knocked down, which was greater in KOH HCT116 cells (about 50% in WTN, KON, and WTH $P < 0.001$ to $P < 0.01$: and 60% in KOH $P < 0.01$; Supplementary Fig. S7A).

HIF1α differentially regulates expression of CK isoenzymes

Metabolic analysis highlighted Cr metabolism as a mechanism that could compensate for loss of HIF1α activity by promoting the reversible reaction PCr+ADP = Cr+ATP. By proteomics analysis, KCRB was upregulated in the absence of HIF1α in both normoxia and hypoxia. KCRU was downregulated in the absence of HIF1α in both normoxia and hypoxia (Figs. 3E and 4C). The expression also correlated with the transcriptomics data (Fig. 4D). These data were then validated by PCR (Fig. 5A and B) and by Western blot analysis (Fig. 5D). These data were confirmed in two additional colorectal cancer cell lines, DLD1, and Ls174T (Supplementary Figs. S4B, S4C, S5B, and S5C). The cytosolic enzyme KCRB was upregulated in the absence of HIF1α and the mitochondrial enzyme KCRU was upregulated in the presence of HIF1α (Fig. 5D). KCRB dimer isoenzyme (KCRBB) activity (measured in whole cell extract) matched protein and mRNA expression (Fig. 5E).

In addition, we found (by PCR analysis) that hypoxia upregulated cell membrane Cr transporter *SLC6A8* equally in WTH and KOH versus normoxia (Fig. 5A and B).

Interestingly, total KCR activity in HCT116 cells showed the same changes as KCRBB (Fig. 5E; Supplementary Fig. S7C). We evaluated total KCR activity also in MCF7 breast cancer cells WT or KO. In normoxia, total MCF7 KCR activity was increased in KON versus WTN, showing a similar effect to HCT116 normoxic experiments. Also, no difference was observed between KON and KOH. However, in contrast, in hypoxia, MCF7 KCR activity increased to the same level as KOH. This could reflect the much lower basal activity observed in this cell line (10 times lower than HCT116; Supplementary Fig. S7B–S7D). Finally, in 337 CODREAD patients with colorectal cancer *KCRU* (*CKMT1A*, and *CKMT1B* mitochondrial genes coding for *KCRU*) correlated positively with hypoxia signatures (Supplementary Fig. S2B).

Creatine metabolism is essential for hypoxic tumor growth in absence of HIF1α

We tested the effect of Cr metabolism on growth by using cyclocreatine (cc) to inhibit Cr kinase enzyme activity and methionine (Met) deprivation, precursor in Cr biosynthesis through the reaction mediated by S-adenosyl-L-methionine/Guanidinoacetate N-methyltransferase. In HCT116, we observed that after cc addition, there was an overall reduction in proliferation in WT and KO in both normoxia and hypoxia (Fig. 6A). In normoxia, Met deprivation significantly reduced cell proliferation. In hypoxia, the effect was less pronounced for KO cells and was not significant for WT HCT116 cells (Fig. 6B), showing compensation by a partially HIF-dependent pathway in hypoxia. We confirmed these results in the clonogenic capability of HCT116 cells with and without cc. Interestingly, only KONcc and KOHcc showed a significant reduction in clone formation with KOHcc substantially lower than KONcc (Fig. 6C and D). Finally, in spheroids, cc decreased the volume in KO-cc treated (day 10) as compared with KO controls (Fig. 6E and F). KCRB knocked down in HCT116 showed a significant reduction of cell proliferation of more than 50% in all experimental conditions (WTN< KON< and WTH $P < 0.00$; KOH $P < 0.01$; Supplementary Fig. S7E). FC in HCT116 cells' proliferation comparing normoxia and hypoxia upon KCRB silencing in HIF1α-deficient and control showed significant reduction in KOH/WTH (FC = 0.2 ± 0.05) compared with KON/WTN (FC = 0.5 ± 0.05, $P < 0.001$), WTH/WTN (FC = 0.3 ± 0.03, $P < 0.05$), and KOH/KON (FC = 0.4 ± 0.05, $P < 0.001$). Altogether, these data confirm the results of cc experiments.

Discussion

In this study, we show how hypoxic cancer cells can metabolically compensate for HIF1α loss in hypoxia. In particular, we identified two main adaptive metabolic processes allowing cancer cells to support and meet their energetic and precursors needs for proliferation in hypoxia in the absence of HIF1α (Fig. 7 summary diagram).

Hypoxic HIF1α-deficient cancer cells maintain a significant proliferation and metabolic capability. Several HIF1α-independent hypoxic responses have been reported to sustain tumor growth via NFκB or PHD1/EglN2 (11–13) and support tumor metabolism via fructose and lipid metabolic pathways (10, 14). As expected, in hypoxia, HIF1α promotes GTR1 expression and a dynamic induction of Glu-6P intracellular gradient increase. This regulation, HIF1α/PI3K/Akt–mediated, ensures glucose supply to high glycolytic proliferating cancer cells (15).

Published OnlineFirst March 18, 2019; DOI: 10.1158/1541-7786.MCR-18-0315

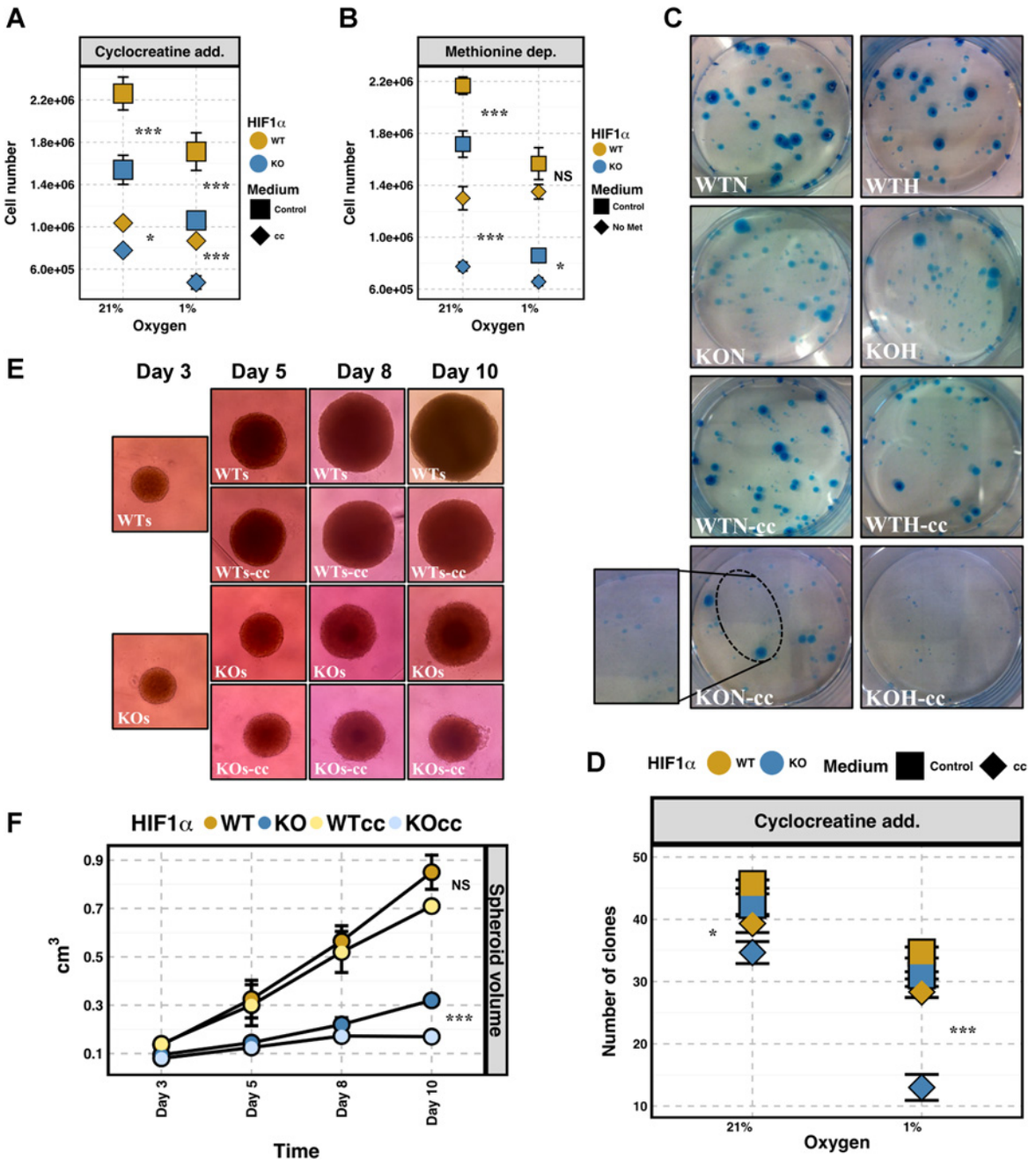

Figure 6.

Creatine metabolism is essential for hypoxic tumor growth in absence of HIF1α. **A,** Effect of cc addition on WTN, KON, WTH, and KOH cells after 24-hour exposure to two O_2 conditions (21% and 1%). **B,** Effect of methionine deprivation on WTN, KON, WTH, and KOH cells after 24-hour exposure to two O_2 conditions (21% and 1%). **C** and **D,** Effect of cc addition on WTN, KON, WTH, and KOH cell clonogenic (number of clones counted) after 24-hour exposure to two O_2 conditions (21% and 1%). **E** and **F,** Effect of cc addition on HCT116 WT and KO spheroid growth (volume) at days 5, 8, and 10 (cc added at day 3 and subsequent days after spheroid formation). Data are reported as average ± SD ($N = 3$). Statistical comparisons were performed using two-way ANOVA, multiple *post hoc* group comparisons, or *t* test (*P* values corrected using the Benjamini–Hochberg procedure at $\alpha = 1\%$), showing *P* value <0.05 (*), <0.01 (**), and <0.001 (***).

However, in the absence of HIF1α, we found that low GTR1 coexisted with a sustained intracellular Glu-6P level in hypoxia. This metabolic phenotype was associated with an induction of GTR3 and GTR14 at mRNA and protein level. GTR3 and GTR14 share 95% nucleotide identity (16), and GTR14 was thought to be a GTR3 variant (17). Indeed, we found that GTR14 antibody detection yielded a signal for both GTR3 and GTR14 proteins, while mass spectrometry analysis did not result in a high enough

Published OnlineFirst March 18, 2019; DOI: 10.1158/1541-7786.MCR-18-0315

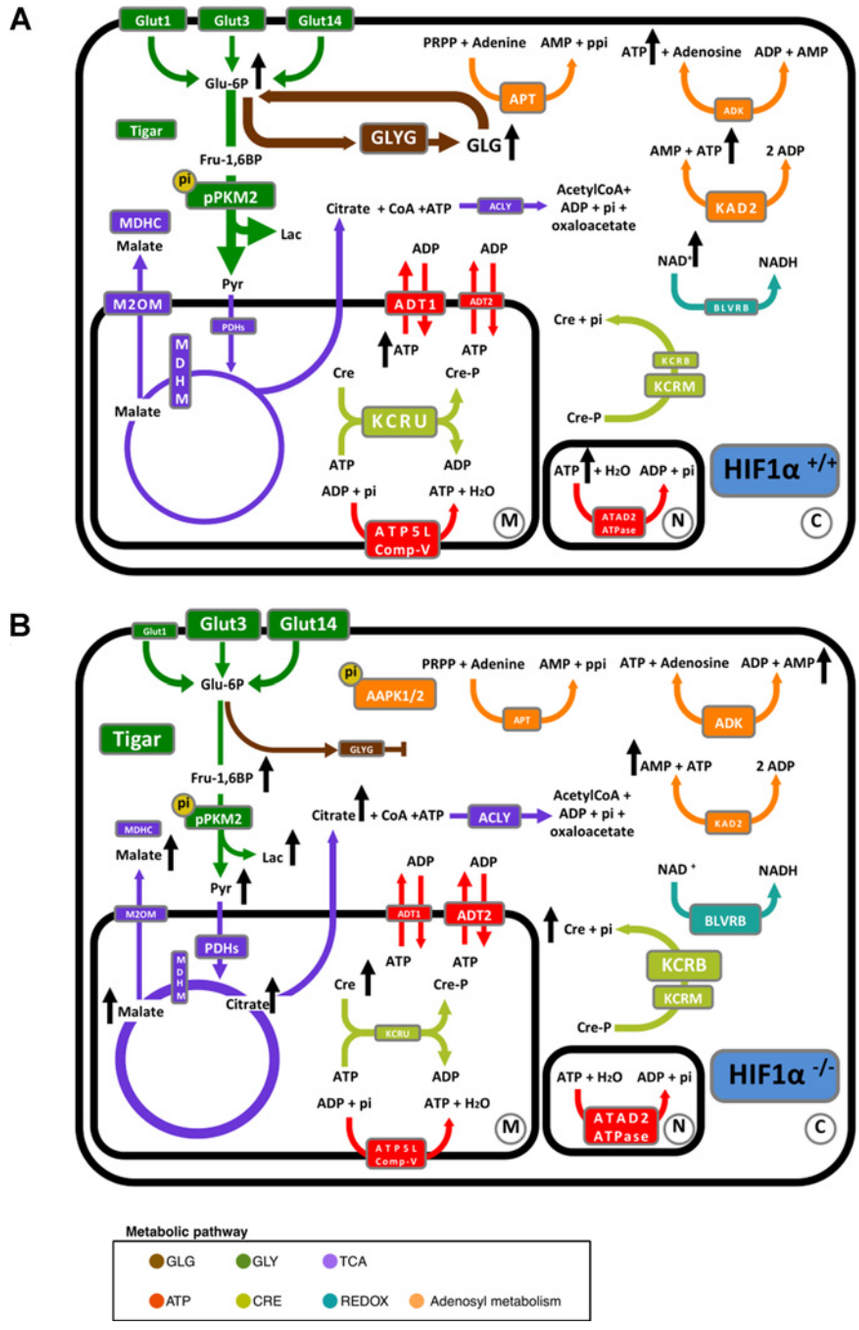

Figure 7.
The metabolic pathways and metabolites described in this study. **A,** Adaptation of hypoxic cancer cell metabolism by HIF1α maintains energetic, redox, and biosynthetic requirements. **B,** In this manuscript, Valli and colleagues reveal for the first time that cancer cell growth and energy metabolism is maintained by HIF1α-independent metabolic pathways under hypoxia that involve glucose uptake by GLUT14 and creatine metabolism. Metabolic pathways: glycogen (GLG), glycolysis (GLY), Krebs cycle (TCA), adenosine triphosphate (ATP), creatine (Cr), oxidation–reduction (REDOX), and adenosyl metabolism. (↑), Increase; (↓), decrease, box size and lines/arrows' thickness describe the regulation in the different conditions.

sequence coverage to discriminate between the two glucose transporters.

Adaptation of cancer cells to local glucose and Cr concentrations occurs by specific regulation of Glu transporters expression, glycolytic enzymes, or ATP levels (18, 19). In our data, GTR3 regulation did not display typical HIF2α dependency although expressed at higher basal levels in the KO cells, it was induced in WT by hypoxia to the same level, suggesting, in this case, another mechanism, for example, NfκB, has replaced HIF1α (20) while GTR14 upregulation was driven by HIF2α in the absence of HIF1α. However, in DLD1, GTR3 is clearly a HIF2 target, showing the variation that can occur in this regulation. Because of the high affinity for Glu, GTR3 overexpression could provide growth advantages in tumors already at low Glu levels (18). Interestingly, a link between hypoxia, GTR3, and Glu uptake was suggested to be important for lipid biosynthesis in macrophages (21). In line with this, HIF2α was reported to play a major role in lipid metabolism (22). GTR14 has been associated with low survival in human testis and in patients with gastric adenocarcinoma (23). Alternative mechanisms by which GTR3 and GTR1 can be regulated include HIF2α via Ptpmt1 and HIF1α via IGF-1, respectively (24, 25). The reason that GTR14KD, but not GT3KD, affects

Published OnlineFirst March 18, 2019; DOI: 10.1158/1541-7786.MCR-18-0315

HCT116 cell proliferation may be related to relative flux through the pathways if GTR14 was the major transporter, or because GTR14 is also a dehydroascorbate transporter (26), but these require further analysis.

HIF1α in hypoxia enhances tumor glycolytic enzymes expression and glycolytic flux (27). In hypoxia, in the absence of HIF1α, we found an accumulation of most of the glycolytic intermediates, which was accompanied by low glycolysis enzymatic levels and glycolytic flux.

Our results match previous data in HCT116 HIF1β KD and hepatoma cancer cells where Glu uptake was maintained in either normoxia or hypoxia despite the downregulation of many glycolytic genes (28) with a mechanism that involved autophagy. An increase of Glu-6P and Fru-1,6BP metabolic flux not only contributes to glycolytic ATP production, but can also provide precursors for auxiliary pathways such as, glycogen, PPP, and lipids (10, 14, 29, 30).

In hypoxia, in the absence of HIF1α, we found a blockage at the metabolic step mediated by fructose-bisphosphate aldolase (Aldolase A, ALDOA), catabolizing the cleavage of Fru-1,6BP to glyceraldehyde 3-phosphate and dihydroxyacetone phosphate. Previously, it has been shown that PFKB3 was key in regulating glycolysis one step earlier, and has been the focus of several approaches to develop inhibitors (31). Our data highlight that ALDOA should be considered as a target for therapy now. ALDOA was shown to stabilize HIF1α via PDH in lung cancer and to promote cancer progression *in vivo* (32, 33). ALDO is activated via PI3K, which recruits ALDO from the cytoskeleton and redistributes it in the cytosol where it can increase glycolysis (34). Finally, ALDOA was shown to be induced by hypoxia in colorectal cancer-derived cell lines and to be an independent prognostic factor for colorectal cancer (35).

In hypoxia, in the presence of HIF1α, we found that Pyr and lactate levels were lower compared with HIF1α KO This could be due to a faster metabolism of Pyr into lactate by LDHA and its subsequent removal through transporters (15). As LDHA and lactate transporters are HIF1α targets, this flux can be reduced in hypoxic HIF1α-deficient cells, thus explaining the observed high intracellular levels found for Pyr and lactate.

We also found that in hypoxia, citrate levels are elevated and Pyr oxidation into the TCA is overall maintained in the absence of HIF1α. Under hypoxic conditions, HIF1α drives phosphorylation of PDK that inhibits PDH and shunts Pyr away from mitochondria to lactate, reducing the rate of oxidative decarboxylation and diminishing acetyl-CoA formation (36). Consequently, replenishment of TCA cycle in mitochondria is altered. In such conditions, citrate biosynthesis is prevented, reductive carboxylation is enhanced, and a HIF1α-dependent mechanism allows hypoxic cells to metabolize glutamine into fatty acids trough citrate formation (37). Consistent with this, the high fully labeled malate content could be due to malate formation associated with a decreased malate transport outside the mitochondria (M2OM) and a reduced metabolism that is MDHM/MDHC-dependent (Fig. 4). Finally, STIR reduction in TCA versus glycolysis (more evident in the presence of HIF1α) shows the metabolic uncoupling that is HIF1α-dependent in hypoxic cancer cells. Our finding that, in hypoxia, fully labeled citrate formation is favored and malate is accumulated in the absence of HIF1α, suggests diminished reductive carboxylation as the predominant metabolic regulation.

In HCT116 spheroids and 2D hypoxic cells, we found a strong increase of AMP levels in absence of HIF1α. This was accompanied by a strong expression of p-AMPK in HCT116 KO cells only. Previous data report AMPK being activated in low-oxygen conditions by a HIF1α-independent mechanism (38), potentially responding to cellular energy status through AMP binding to AMPK γ subunit, so promoting phosphorylation by upstream kinases and finally inhibiting AMPK dephosphorylation (39). In addition, in our results intracellular ATP levels were higher in the presence of HIF1α, although ATP is maintained in its absence. This was found to be consistent with a generally reduced protein synthesis (as assessed by mRNA/protein ratios) as this process is a primary energy-consuming process that can account for up to 70% of cellular ATP utilization (40). Under hypoxia, a rapid inhibition of global mRNA translation represents a major protective strategy to maintain energy (41).

However, ATP maintenance is a process linked to ATP re/generating metabolic systems that relies on biochemical regulatory systems at subcellular level (42). For example, in skeletal muscle, the high availability of PCr and Cr allows ATP maintenance by promoting the reversible reaction PCr+ADP = Cr+ATP. The Cr kinase system, highly expressed in human tissues with high-energy demand, can enhance neuromuscular performance on an anaerobic short extent and during anaerobic intermittent exercise (43). Indeed, active skeletal muscles capable of ATP anaerobic biosynthesis keep global ATP reasonably constant during exercise.

This is accomplished by the Cr kinase metabolic system that replenishes the rate of ATP use at a fast pace (44). HIF2α-modulated hypoxic response elements have been reported to be involved in Cr metabolism (45). Interestingly, our study shows that both in normoxia and hypoxia, HIF1α maintains levels of the mitochondrial CK isoenzyme, KCRU, which was associated with a reduced TCA cycle. In contrast, the cytoplasmic CK isoenzyme, KCRB, is lower in WT cells. Strikingly, in cells without HIF1α, this distribution was reversed, irrespective of hypoxia. This shows the importance of low levels of HIF1α expression in regulating metabolic pathways. The complex effects of altering these enzymes on cell survival is shown by KCRU overexpression, which enhanced the survival of breast cancer cells, while KCRB KD induced cell death in hypoxic ovarian cancer cells (43). Cr metabolism, which translocates ATP from sites of production to locations of ATP consumption, acts as a spatial/temporal energy buffer utilizing Cr, ATP, and ADP at distinct subcellular compartments (46). Consistent with this, colon cancer cells were shown to secrete KCRB extracellularly to generate and import PCr to enhance energy (19). KCRB and KCRM genes emerged as HIF2α-selective targets, and regulation of Cr kinase by HIF was shown in the gut (46), suggesting a role for HIF2α in energy maintenance. In the absence of HIF1α, we found that cc reduces HCT116 cells' clonogenic capability and spheroid volume. KCRB depletion/inhibition in combination with chemotherapeutic agents showed synergistic effects in cancer therapy (47). Cr kinase metabolic inhibition by cc was shown to decrease cell viability, promote cell-cycle arrest, and apoptosis in EVI1 (48). Inhibition of the colon cancer cell line KCRB by preincubation with cc reduced liver metastasis formation and depleted PCr (49) and recently, mice inoculated with colorectal cancer cells and treated with cc showed a significant reduction in metastatic colonization (19). Our novel experimental work has shown that silencing of GTR14 or KCRB reduces the proliferation rate of HIF1α-KO

HCT116 cells in normoxic and hypoxic conditions. Because GRT14 and KCRB are more highly expressed in HIF1α-KO hypoxic HCT116 cells, silencing these genes alters in a larger extent HCT116 HIF1α-KO cells' proliferation in hypoxia than control.

In summary, our work shows for the first time that hypoxic cancer cells harbor the capability to compensate for HIF1α-deficient metabolic impasses by inducing GTR14-mediated Glu internalization in a HIF1α/HIF2α antagonistic fashion. We also report Cr metabolism is tuned to function as a fast ATP buffering biochemical system. Aldolase A is shown to be a control point in glycolysis by HIF1α. As these alternate metabolic pathways were shown for the first time in 3D cancer cell cultures, they provide a model relevant to micrometastases and drug targeting. Under hypoxia and HIF1 blockade, cancer cells adapt their energy metabolism via upregulation of the GLUT14 glucose transporter and creatine metabolism providing new avenues for drug targeting.

Disclosure of Potential Conflicts of Interest

No potential conflicts of interest were disclosed.

Authors' Contributions

Conception and design: A. Valli, A. McIntyre, B.M. Kessler, A.L. Harris
Development of methodology: A. Valli, D. Baban, M. Rodriguez, S. Zervou
Acquisition of data (provided animals, acquired and managed patients, provided facilities, etc.): A. Valli, M. Morotti, C.E. Zois, T. Soga, K. Feldinger, R. Fischer, A. McIntyre, E. Bridges, D. Baban, M. Rodriguez, O. Yanes, H.J. Whittington, H.A. Lake, C.A. Lygate
Analysis and interpretation of data (e.g., statistical analysis, biostatistics, computational analysis): A. Valli, P.K. Albers, K. Feldinger, R. Fischer, M. Frejno, S. Haider, F.M. Buffa, D. Baban, O. Yanes, H.A. Lake, S. Zervou, C.A. Lygate, B.M. Kessler, A.L. Harris
Writing, review, and/or revision of the manuscript: A. Valli, M. Morotti, R. Fischer, A. McIntyre, O. Yanes, C.A. Lygate, B.M. Kessler, A.L. Harris
Administrative, technical, or material support (i.e., reporting or organizing data, constructing databases): A. Valli, E. Bridges, D. Baban, A.L. Harris
Study supervision: A. Valli, F.M. Buffa, B.M. Kessler, A.L. Harris
Other (conducted experiments): C.E. Zois

Acknowledgments

This work was supported by a Cancer Research UK (CRUK) program grant (C602/A18974, to A.L. Harris). B.M. Kessler is supported by the Biomedical Research Centre (NIHR) Oxford, United Kingdom. C.A. Lygate is supported by British Heart Foundation Programme Grant (RG/13/8/30266).

The costs of publication of this article were defrayed in part by the payment of page charges. This article must therefore be hereby marked *advertisement* in accordance with 18 U.S.C. Section 1734 solely to indicate this fact.

Received March 30, 2018; revised January 28, 2019; accepted March 13, 2019; published first March 18, 2019.

References

1. Vander Heiden MG, Cantley LC, Thompson CB. Understanding the Warburg effect: the metabolic requirements of cell proliferation. Science 2009;324:1029–33.
2. Warburg O, Wind F, Negelein E. The metabolism of tumors in the body. J Gen Physiol 1927;8:519–30.
3. Pfeiffer T, Schuster S, Bonhoeffer S. Cooperation and competition in the evolution of ATP-producing pathways. Science 2001;292:504–7.
4. Eidelman E, Twum-Ampofo J, Ansari J, Siddiqui MM. The metabolic phenotype of prostate cancer. Front Oncol 2017;7:131.
5. Palmer CS, Cherry CL, Sada-Ovalle I, Singh A, Crowe SM. Glucose metabolism in T cells and monocytes: new perspectives in HIV pathogenesis. EBioMedicine 2016;6:31–41.
6. Pavlova NN, Thompson CB. The emerging hallmarks of cancer metabolism. Cell Metab 2016;23:27–47.
7. Liberti MV, Locasale JW. The Warburg effect: how does it benefit cancer cells? Trends Biochem Sci 2016;41:211–8.
8. Xie H, Simon MC. Oxygen availability and metabolic reprogramming in cancer. J Biol Chem 2017;292:16825–32.
9. Mole DR, Blancher C, Copley RR, Pollard PJ, Gleadle JM, Ragoussis J, et al. Genome-wide association of hypoxia-inducible factor (HIF)-1alpha and HIF-2alpha DNA binding with expression profiling of hypoxia-inducible transcripts. J Biol Chem 2009;284:16767–75.
10. Valli A, Rodriguez M, Moutsianas L, Fischer R, Fedele V, Huang HL, et al. Hypoxia induces a lipogenic cancer cell phenotype via HIF1alpha-dependent and -independent pathways. Oncotarget 2015;6:1920–41.
11. Klein O, Rohwer N, de Molina KF, Mergler S, Wessendorf P, Herrmann M, et al. Application of two-dimensional gel-based mass spectrometry to functionally dissect resistance to targeted cancer therapy. Proteomics Clin Appl 2013;7:813–24.
12. Rohwer N, Bindel F, Grimm C, Lin SJ, Wappler J, Klinger B, et al. Annexin A1 sustains tumor metabolism and cellular proliferation upon stable loss of HIF1A. Oncotarget 2016;7:6693–710.
13. Li Y, Padmanabha D, Gentile LB, Dumur CI, Beckstead RB, Baker KD. HIF- and non-HIF-regulated hypoxic responses require the estrogen-related receptor in Drosophila melanogaster. PLoS Genet 2013;9:e1003230.
14. Armitage EG, Kotze HL, Allwood JW, Dunn WB, Goodacre R, Williams KJ. Metabolic profiling reveals potential metabolic markers associated with Hypoxia Inducible Factor-mediated signalling in hypoxic cancer cells. Sci Rep 2015;5:15649.
15. Schulze A, Harris AL. How cancer metabolism is tuned for proliferation and vulnerable to disruption. Nature 2012;491:364–73.
16. Augustin R. The protein family of glucose transport facilitators: it's not only about glucose after all. IUBMB Life 2010;62:315–33.
17. Schlosser HA, Drebber U, Urbanski A, Haase S, Baltin C, Berlth F, et al. Glucose transporters 1, 3, 6, and 10 are expressed in gastric cancer and glucose transporter 3 is associated with UICC stage and survival. Gastric Cancer 2015;20:83–91.
18. Birsoy K, Possemato R, Lorbeer FK, Bayraktar EC, Thiru P, Yucel B, et al. Metabolic determinants of cancer cell sensitivity to glucose limitation and biguanides. Nature 2014;508:108–12.
19. Loo JM, Scherl A, Nguyen A, Man FY, Weinberg E, Zeng Z, et al. Extracellular metabolic energetics can promote cancer progression. Cell 2015;160:393–406.
20. Christensen DR, Calder PC, Houghton FD. GLUT3 and PKM2 regulate OCT4 expression and support the hypoxic culture of human embryonic stem cells. Sci Rep 2015;5:17500.
21. Li L, Liu B, Haversen L, Lu E, Magnusson LU, Stahlman M, et al. The importance of GLUT3 for de novo lipogenesis in hypoxia-induced lipid loading of human macrophages. PLoS One 2012;7:e42360.
22. Rankin EB, Rha J, Selak MA, Unger TL, Keith B, Liu Q, et al. Hypoxia-inducible factor 2 regulates hepatic lipid metabolism. Mol Cell Biol 2009;29:4527–38.
23. Berlth F, Monig S, Pinther B, Grimminger P, Maus M, Schlosser H, et al. Both GLUT-1 and GLUT-14 are independent prognostic factors in gastric adenocarcinoma. Ann Surg Oncol 2015;22Suppl 3:S822–31.
24. Xu QQ, Xiao FJ, Sun HY, Shi XF, Wang H, Yang YF, et al. Ptpmt1 induced by HIF-2alpha regulates the proliferation and glucose metabolism in erythroleukemia cells. Biochem Biophys Res Commun 2016;471:459–65.
25. Yu J, Li J, Zhang S, Xu X, Zheng M, Jiang G, et al. IGF-1 induces hypoxia-inducible factor 1alpha-mediated GLUT3 expression through PI3K/Akt/mTOR dependent pathways in PC12 cells. Brain Res 2012;1430:18–24.
26. Amir Shaghaghi M, Zhouyao H, Tu H, El-Gabalawy H, Crow GH, Levine M, et al. The SLC2A14 gene, encoding the novel glucose/dehydroascorbate transporter GLUT14, is associated with inflammatory bowel disease. Am J Clin Nutr 2017;106:1508–13.
27. Marin-Hernandez A, Gallardo-Perez JC, Ralph SJ, Rodriguez-Enriquez S, Moreno-Sanchez R. HIF-1alpha modulates energy metabolism in cancer

cells by inducing over-expression of specific glycolytic isoforms. Mini Rev Med Chem 2009;9:1084–101.
28. Frezza C, Zheng L, Tennant DA, Papkovsky DB, Hedley BA, Kalna G, et al. Metabolic profiling of hypoxic cells revealed a catabolic signature required for cell survival. PLoS One 2011;6:e24411.
29. Favaro E, Bensaad K, Chong MG, Tennant DA, Ferguson DJ, Snell C, et al. Glucose utilization via glycogen phosphorylase sustains proliferation and prevents premature senescence in cancer cells. Cell Metab 2012;16:751–64.
30. Bensaad K, Favaro E, Lewis CA, Peck B, Lord S, Collins JM, et al. Fatty acid uptake and lipid storage induced by HIF-1alpha contribute to cell growth and survival after hypoxia-reoxygenation. Cell Rep 2014;9:349–65.
31. Lu L, Chen Y, Zhu Y. The molecular basis of targeting PFKFB3 as a therapeutic strategy against cancer. Oncotarget 2017;8:62793–802.
32. Chang YC, Chan YC, Chang WM, Lin YF, Yang CJ, Su CY, et al. Feedback regulation of ALDOA activates the HIF-1alpha/MMP9 axis to promote lung cancer progression. Cancer Lett 2017;403:28–36.
33. Sanzey M, Abdul Rahim SA, Oudin A, Dirkse A, Kaoma T, Vallar L, et al. Comprehensive analysis of glycolytic enzymes as therapeutic targets in the treatment of glioblastoma. PLoS One 2015;10:e0123544.
34. Hu H, Juvekar A, Lyssiotis CA, Lien EC, Albeck JG, Oh D, et al. Phosphoinositide 3-kinase regulates glycolysis through mobilization of aldolase from the actin cytoskeleton. Cell 2016;164:433–46.
35. Kawai K, Uemura M, Munakata K, Takahashi H, Haraguchi N, Nishimura J, et al. Fructose-bisphosphate aldolase A is a key regulator of hypoxic adaptation in colorectal cancer cells and involved in treatment resistance and poor prognosis. Int J Oncol 2017;50:525–34.
36. Kim JW, Tchernyshyov I, Semenza GL, Dang CV. HIF-1-mediated expression of pyruvate dehydrogenase kinase: a metabolic switch required for cellular adaptation to hypoxia. Cell Metab 2006;3:177–85.
37. Metallo CM, Gameiro PA, Bell EL, Mattaini KR, Yang J, Hiller K, et al. Reductive glutamine metabolism by IDH1 mediates lipogenesis under hypoxia. Nature 2011;481:380–4.
38. Laderoute KR, Amin K, Calaoagan JM, Knapp M, Le T, Orduna J, et al. 5′-AMP-activated protein kinase (AMPK) is induced by low-oxygen and glucose deprivation conditions found in solid-tumor microenvironments. Mol Cell Biol 2006;26:5336–47.
39. Li YH, Luo J, Mosley YY, Hedrick VE, Paul LN, Chang J, et al. AMP-Activated protein kinase directly phosphorylates and destabilizes Hedgehog pathway transcription factor GLI1 in medulloblastoma. Cell Rep 2015;12:599–609.
40. Koritzinsky M, Wouters BG. Hypoxia and regulation of messenger RNA translation. Methods Enzymol 2007;435:247–73.
41. Staudacher JJ, Naarmann-de Vries IS, Ujvari SJ, Klinger B, Kasim M, Benko E, et al. Hypoxia-induced gene expression results from selective mRNA partitioning to the endoplasmic reticulum. Nucleic Acids Res 2015;43:3219–36.
42. Kazak L, Chouchani ET, Jedrychowski MP, Erickson BK, Shinoda K, Cohen P, et al. A creatine-driven substrate cycle enhances energy expenditure and thermogenesis in beige fat. Cell 2015;163:643–55.
43. Yan YB. Creatine kinase in cell cycle regulation and cancer. Amino Acids 2016;48:1775–84.
44. Khan JR, Iftikar FI, Herbert NA, Gnaiger E, Hickey AJ. Thermal plasticity of skeletal muscle mitochondrial activity and whole animal respiration in a common intertidal triplefin fish, Forsterygion lapillum (Family: Tripterygiidae). J Comp Physiol B 2014;184:991–1001.
45. Zheng L, Kelly CJ, Colgan SP. Physiologic hypoxia and oxygen homeostasis in the healthy intestine. A review in the theme: cellular responses to hypoxia. Am J Physiol Cell Physiol 2015;309:C350–60.
46. Kitzenberg D, Colgan SP, Glover LE. Creatine kinase in ischemic and inflammatory disorders. Clin Transl Med 2016;5:31.
47. Li XH, Chen XJ, Ou WB, Zhang Q, Lv ZR, Zhan Y, et al. Knockdown of creatine kinase B inhibits ovarian cancer progression by decreasing glycolysis. Int J Biochem Cell Biol 2013;45:979–86.
48. Fenouille N, Bassil CF, Ben-Sahra I, Benajiba L, Alexe G, Ramos A, et al. The creatine kinase pathway is a metabolic vulnerability in EVI1-positive acute myeloid leukemia. Nat Med 2017;23:301–13.
49. Lillie JW, O'Keefe M, Valinski H, Hamlin HA Jr, Varban ML, Kaddurah-Daouk R. Cyclocreatine (1-carboxymethyl-2-iminoimidazolidine) inhibits growth of a broad spectrum of cancer cells derived from solid tumors. Cancer Res 1993;53:3172–8.

Published OnlineFirst March 18, 2019; DOI: 10.1158/1541-7786.MCR-18-0315

American Association for Cancer Research

Molecular Cancer Research

Adaptation to HIF1α Deletion in Hypoxic Cancer Cells by Upregulation of GLUT14 and Creatine Metabolism

Alessandro Valli, Matteo Morotti, Christos E. Zois, et al.

Mol Cancer Res 2019;17:1531-1544. Published OnlineFirst March 18, 2019.